

Research



Cite this article: Li Q, Kartikowati CW, Iwaki T, Okuyama K, Ogi T. 2020 Enhanced magnetic performance of aligned wires assembled from nanoparticles: from nanoscale to macroscale. *R. Soc. Open Sci.* **7**: 191656. <http://dx.doi.org/10.1098/rsos.191656>

Received: 19 September 2019

Accepted: 26 March 2020

Subject Category:

Chemistry

Subject Areas:

nanotechnology

Keywords:

magnetic wire, nanoparticle assembly, parallel arrays

Author for correspondence:

Takashi Ogi

e-mail: ogit@hiroshima-u.ac.jp

This article has been edited by the Royal Society of Chemistry, including the commissioning, peer review process and editorial aspects up to the point of acceptance.

Electronic supplementary material is available online at <https://doi.org/10.6084/m9.figshare.c.4936716>.



Enhanced magnetic performance of aligned wires assembled from nanoparticles: from nanoscale to macroscale

Qing Li¹, Christina W. Kartikowati², Toru Iwaki³, Kikuo Okuyama³ and Takashi Ogi³

¹Department of Environmental Science and Engineering, Fudan University, Shanghai 200433, People's Republic of China

²Jurusan Teknik Kimia, Fakultas Teknik, Universitas Brawijaya, Jl. MT. Haryono 167, Malang 65145, Indonesia

³Department of Chemical Engineering, Graduate School of Engineering, Hiroshima University, 1-4-1 Kagamiyama, Higashi, Hiroshima 739-8527, Japan

QL, 0000-0003-0587-1748; CWK, 0000-0001-5288-0378; KO, 0000-0002-1477-1442; TO, 0000-0003-3982-857X

Magnetic wires in highly dense arrays, possessing unique magnetic properties, are eagerly anticipated for inexpensive and scalable fabrication technologies. This study reports a facile method to fabricate arrays of magnetic wires directly assembled from well-dispersed α'' -Fe₁₆N₂/Al₂O₃ and Fe₃O₄ nanoparticles with average diameters of 45 nm and 65 nm, respectively. The magnetic arrays with a height scale of the order of 10 nm were formed on substrate surfaces, which were perpendicular to an applied magnetic field of 15 T. The applied magnetic field aligned the easy axis of the magnetic nanoparticles (MNPs) and resulted in a significant enhancement of the magnetic performance. Hysteresis curves reveal that values of magnetic coercivity and remanent magnetization in the preferred magnetization direction are both higher than that of the nanoparticles, while these values in the perpendicular direction are both lower. Enhancement in the magnetic property for arrays made from spindle-shape α'' -Fe₁₆N₂/Al₂O₃ nanoparticles is higher than that made from cube-like α'' -Fe₁₆N₂/Al₂O₃ ones, owing to the shape anisotropy of MNPs. Furthermore, the assembled highly magnetic α'' -Fe₁₆N₂/Al₂O₃ arrays produced a detectable magnetic field with an intensity of approximately 0.2 T. Although high-intensity external field benefits for the fabrication of magnetic arrays, the newly developed technique provides an environmentally friendly and feasible approach to fabricate magnetic wires in highly dense arrays in open environment condition.

1. Introduction

Magnetic wire-like structures with high aspect ratios, a link between nanoscale objects and the macroscale world, play important roles in both fundamental research and the development of modern materials [1,2]. The high aspect ratio endows the material with anisotropic properties and ensures that magnetization prefers to align with the long axis of the wires [3–5]. A longitudinal magnetic anisotropy has been widely reported to be related to strong shape anisotropy because the coercive fields in the wire direction are lower than those perpendicular to it [4,6–8]. Anisotropic magnetic wires also have higher magnetic moments than their spherical counterparts and therefore open up new possibilities for applications [5,9]. As a consequence, magnetic wire-like structures are of great interest in the development of new-generation spintronic devices [3], sensors [10], data storage technologies [11–13], biological and harsh environment applications [7,14], as well as many other potential applications [1,5,15]. To exploit their collective properties and the various applications in functional devices, many methods have been developed to produce wire-like structures [1,16].

The approaches used to obtain high aspect ratio magnetic wires can be generally classified into two main categories, i.e. direct synthesis and assembly methods [5]. The direct synthesis method includes solid-state, vapour-phase and liquid-/solution-based technique [1]. The solid-state and vapour-phase techniques are commonly costly and require complicated equipment [17,18]. The liquid-/solution-based synthesis technique, also known as a wet chemical process, is a prospective method in terms of applications with relatively low cost, simple equipment and high yield [1,19–21]. However, the morphology of particles, including the aspect ratio, always needs appropriate templates [22–27] or via chemical processes by tuning synthetic conditions, such as temperature, reaction time and reaction media, as well as the ratio and concentration of reagents [28,29]. The template-based method associates with its high cost and time-consuming nature, this method still cannot be adopted for large-scale production [1,30]. Although chemical process method is relatively low-cost and simple, some reaction parameters, including temperature and pH, as well as an external magnetic field (EMF), must be strictly controlled [8,18,31–33].

The assembly method commonly involves the cooperative combination of the EMF and a polymer, responsible for the self-assembly process of magnetic nanoparticles (MNPs) and gluing together the aligned nanoparticles, respectively [5]. EMF-assisted self-assembly of wire structures from MNPs is a simple, low-cost and environmentally friendly method, feasible for application in large-scale production [1,19,34–37]. The self-assembly is directed by an EMF via controlling the magnetic dipole–dipole interaction between MNPs [37–41]. The assembly is commonly performed in a solvent or during a solvent evaporation process to ensure that the MNPs have enough mobility to assemble [15]. A polymer is commonly employed to act as a linker for stabilizing the building blocks and retain the MNPs in the wire-like shape [42]. The combination of an EMF-assisted alignment and a polymer in solution can produce dense wire arrays after solvent evaporation [43]. Owing to the polymer stabilization and the strong interaction between MNPs, the assembled arrays and/or wire-like structures can remain stable when the EMF is removed [2]. The property and morphology of wire-like structures are influenced by several factors, including the EMF, the composition of the solvent and polymers, the pH of solutions and the reaction temperature. Among these, the EMF strength is the most crucial parameter for the formation of wires [1]. However, there are rare studies on the EMF-assisted wires from MNPs directly, especially under strong EMF. Our group succeeded in the rough alignment of core–shell α'' -Fe₁₆N₂ and Fe₃O₄ MNPs in the form of fibres and films, respectively, via magneto-electrospray under a 0.1 T EMF [44,45].

With the aim of fabricating magnetic wires in highly dense arrays, this study reports the magnetic wires directly assembled under 15 T EMF from the well-dispersed core–shell α'' -Fe₁₆N₂/Al₂O₃ and cube-like Fe₃O₄ MNPs with high and low magnetic isotropies, respectively, as well as the core–shell spindle-shaped α'' -Fe₁₆N₂/Al₂O₃ MNPs. We tried to investigate the shape factor of α'' -Fe₁₆N₂/Al₂O₃ NPs and develop the highly orientated α'' -Fe₁₆N₂/Al₂O₃ NPs assembly by applying the high magnetic field to enhance the magnetic performance by comparing with that of dispersed MNP without assembly. Magnetic properties and morphological characteristics of the obtained dense arrays were evaluated in detail and discussed involving the assembly mechanism and the effect of shape anisotropy.

2. Material and methods

2.1. Materials

The core–shell α'' -Fe₁₆N₂/Al₂O₃ and cube-like Fe₃O₄ MNPs with average diameters of 70 and 65 nm were used as the raw materials for the fabrication of magnetic wires in this study. The core–shell

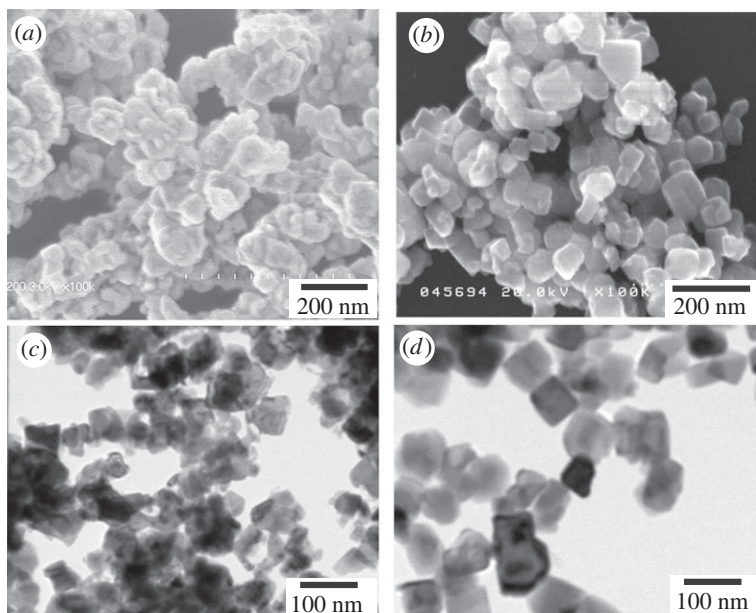


Figure 1. SEM images of core-shell $\alpha''\text{-Fe}_{16}\text{N}_2/\text{Al}_2\text{O}_3$ and cube-like Fe_3O_4 MNPs: (a) $\alpha''\text{-Fe}_{16}\text{N}_2/\text{Al}_2\text{O}_3$ and (b) Fe_3O_4 MNPs before dispersion; (c) $\alpha''\text{-Fe}_{16}\text{N}_2/\text{Al}_2\text{O}_3$ and (d) Fe_3O_4 MNPs after dispersion.

$\alpha''\text{-Fe}_{16}\text{N}_2/\text{Al}_2\text{O}_3$ MNPs with a shell thickness of 4.8 nm were prepared from cube-like Fe_3O_4 MNPs by the surface coating of Al_2O_3 , reduction with H_2 gas and then nitridation with NH_3 gas, as detailed elsewhere [46]. The Fe_3O_4 MNPs with cube-like structures were prepared via a large-scale liquid precipitation method (US Patent no. 5843610, Toda Kogyo Co. Ltd, Japan) as described in our previous report [47]. An epoxy resin (3,4-epoxycyclohexylmethyl 3,4-epoxycyclohexanecarboxylate) was used as an MNP binder.

The colloidal dispersion of MNPs was prepared by using the bead-mill dispersion apparatus (dual axial type bead-mill, Kotobuki Industries, Co. Ltd, Japan), as described in our previous papers [48,49]. The precursor solutions for the wire fabrication were made from the mixture of epoxy resin (1.0 wt%) and MNPs (1.5 wt%) suspended in toluene with NH_4OH added to adjust the pH to approximately 9. Scanning electron microscope (SEM) images for core-shell $\alpha''\text{-Fe}_{16}\text{N}_2/\text{Al}_2\text{O}_3$ and Fe_3O_4 and MNPs before and after dispersion are shown in figure 1. Although the dispersion process was well controlled, sizes of $\alpha''\text{-Fe}_{16}\text{N}_2/\text{Al}_2\text{O}_3$ MNPs were still decreased after dispersion owing to their strong aggregation effect. Average diameters after dispersion are 45.3 and 64.7 nm for $\alpha''\text{-Fe}_{16}\text{N}_2/\text{Al}_2\text{O}_3$ and Fe_3O_4 MNPs, respectively. To determine the implications of the results obtained in this study, spindle-shaped core-shell $\alpha''\text{-Fe}_{16}\text{N}_2/\text{Al}_2\text{O}_3$ MNPs 110 nm in length and 18 nm in width (detailed characteristics were reported in our previous paper [46]) were also used to fabricate wires to reveal the effect of shape anisotropy.

2.2. Fabrication technique

The precursor solutions with the MNP suspension were shaken in an ultrasonic bath (Sine Sonic UA-100, 36 kHz, 100 W) for 30 min before fabrication. The solutions with a volume of 30 ml were then transferred into quartz beakers with inner diameters of 35 mm and inner heights of 15 mm. The beaker was fixed to another quartz beaker, with an inner diameter of 45 mm, a sieve mesh bottom and a hood. The hood was connected to a flexible tube for pumping nitrogen gas with a constant flow rate of 1 l min^{-1} , which was controlled by a mass flow meter. The input of nitrogen gas assisted the evaporation of the solvent in the precursor solutions and flowed out from the bottom of the outside beaker. The packed beaker system, including the solutions, was placed at the centre position of a superconducting magnet (Oxford Instruments, Spectromag-1000) through a bore tube (50 mm). A holder was placed at the bottom of the outside beaker to fix the packed system, as shown in figure 2a. The maximum strength of the EMF was 15.0 T in the vertical direction at the centre position. A detailed description of the superconducting magnet system has been reported elsewhere with the magnetic field spatial distribution along the centre axis shown in figure 2b [50]. The solutions were maintained in the strong

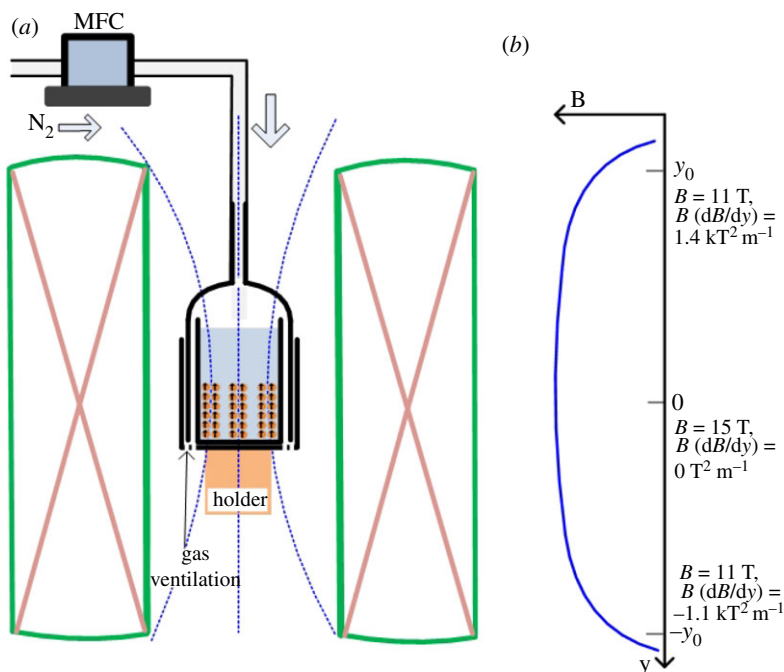


Figure 2. (a) Cross-section of the magnet and schematic illustration of the fabrication process of magnetic wire arrays from MNPs under an EMF of 15 T. (b) Spatial distribution of the magnetic flux density along the vertical axis in the centre of the magnet.

EMF for 24 h evaporation. The whole fabrication process was operated at room temperature, approximately 25°C . Obtained dried wire arrays were scratched for further characterization. Another fabrication via the same method for spindle-shaped core-shell $\alpha''\text{-Fe}_{16}\text{N}_2/\text{Al}_2\text{O}_3$ MNPs was performed under 0.8 T. The 0.8 T was created at the surface centre of a permanent magnet, which was the only dependable and available one in the laboratory.

2.3. Characterization

The morphologies of the MNPs and the fabricated arrays were observed using an SEM (Hitachi S-5000, Japan). Their crystalline structures were examined using X-ray diffraction (XRD; D2 Phaser, Bruker, Germany), while assigned Miller indices of the peaks were obtained from the JCPDS database. Their magnetic properties were evaluated using a superconducting quantum interference device (SQUID, Quantum Design, Tokyo, Japan), which was operated at 300 K. Magnetization was measured as a function of the applied field from 0 to 50 kOe.

3. Results

3.1. Morphology and crystalline structure

Figure 3 presents typical SEM images of the fabricated arrays assembled from core-shell $\alpha''\text{-Fe}_{16}\text{N}_2/\text{Al}_2\text{O}_3$ (figure 3*a-d*) and cube-like Fe_3O_4 MNPs (figure 3*e,f*) under the EMF of 15.0 T. The highly aligned wires are composed of MNPs, as shown in the gradual magnification of wire SEM images from (figure 3*a-d*). The well-dispersed single-domain sized $\alpha''\text{-Fe}_{16}\text{N}_2/\text{Al}_2\text{O}_3$ MNPs participated in the formation of wires along the EMF direction (figure 1*c*). Different from previous nanowires assembled through dipolar interactions between single-domain MNPs and with the same diameter of single-domain MNPs [35,51,52], the assembled wires in this study were not single MNP chains and contained many MNPs in the cross-section of every single wire. Thus, the average diameter of the wires was larger than that of the composite MNPs. The diameters of wires, of the order of $1 \mu\text{m}$, are difficult to estimate because they are overlapped with each other. The average length of the assembled wires is estimated to be approximately 10 mm. Therefore, the ratio between length and width is of the order of 10^4 . The microscope images show that the assembled wires were nearly straight and parallel to each other.

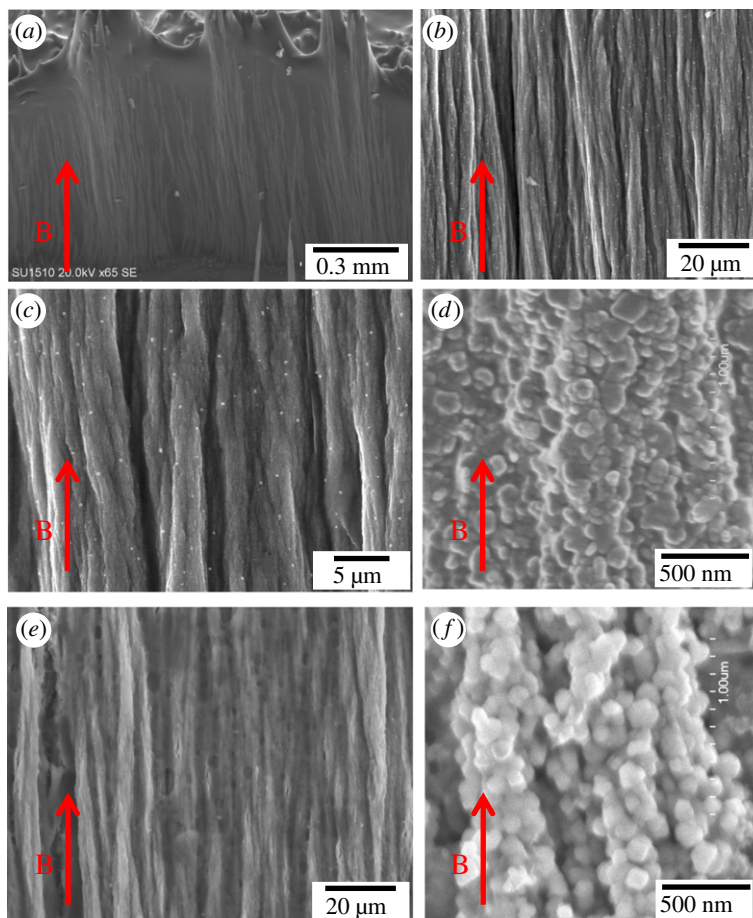


Figure 3. SEM images with different magnifications of fabricated arrays assembled from (a–d) core–shell α'' - $\text{Fe}_{16}\text{N}_2/\text{Al}_2\text{O}_3$ MNPs and (e,f) Fe_3O_4 MNPs under an EMF of 15 T.

Figure 4 shows the XRD patterns of dispersed MNPs, featuring α'' - $\text{Fe}_{16}\text{N}_2/\text{Al}_2\text{O}_3$ and Fe_3O_4 crystalline structures, and those of their assembled arrays under an EMF of 15.0 T. Different from MNPs, the XRD patterns of the fabricated arrays possess a slightly uphill baseline and obvious noise on baselines. This difference probably originates from the addition of the epoxy resin during the production of arrays. Similar phenomena were also observed for fabricating α'' - Fe_{16}N_2 contained fibre sand carbon nanotube films in our previous studies [44,53,54]. The XRD peaks of (202), (220), (004) and (400) from crystalline α'' - $\text{Fe}_{16}\text{N}_2/\text{Al}_2\text{O}_3$ MNPs are also visible for their assembled arrays in the 2θ range of 25° – 70° , while peaks of (111), (311), (222), (400), (422), (511) and (400) from single-crystalline Fe_3O_4 MNPs (as reported in our previous paper [47]) are shown for their assembled arrays in the same 2θ range. The patterns indicate that the fabricated arrays retained the inherent crystalline properties of their composite MNPs.

For the highly magnetic isotropic α'' - Fe_{16}N_2 MNPs and their arrays, the (004) peak has a vertical direction along the c -axis direction, while the (220) peak is in the horizontal direction [54]. When the EMF was applied along the array direction, the (004) and (220) diffraction peaks increased and decreased in the array direction, respectively. The XRD patterns were obtained in the parallel direction of the arrays. By contrast, the (004) and (220) diffraction peaks decreased and increased in the vertical direction of the arrays, respectively, as shown in figure 4. This result is consistent with our previous report on α'' - $\text{Fe}_{16}\text{N}_2/\text{Al}_2\text{O}_3$ films synthesized under various EMF conditions [54]. Therefore, the XRD patterns suggest that the strong EMF leads to increasing the alignment of the c -axis of the MNPs in the array direction.

For the Fe_3O_4 MNPs with low magnetic anisotropy, the (311) plane is in the vertical direction of the c -axis [55]. Similar to the effect of the EMF on the XRD patterns of α'' - $\text{Fe}_{16}\text{N}_2/\text{Al}_2\text{O}_3$ wires, the (311) peak decreased in the vertical direction of arrays, as shown in figure 4. This observation further identifies the effect of the EMF on the alignment of the c -axis of the MNPs in the array direction.

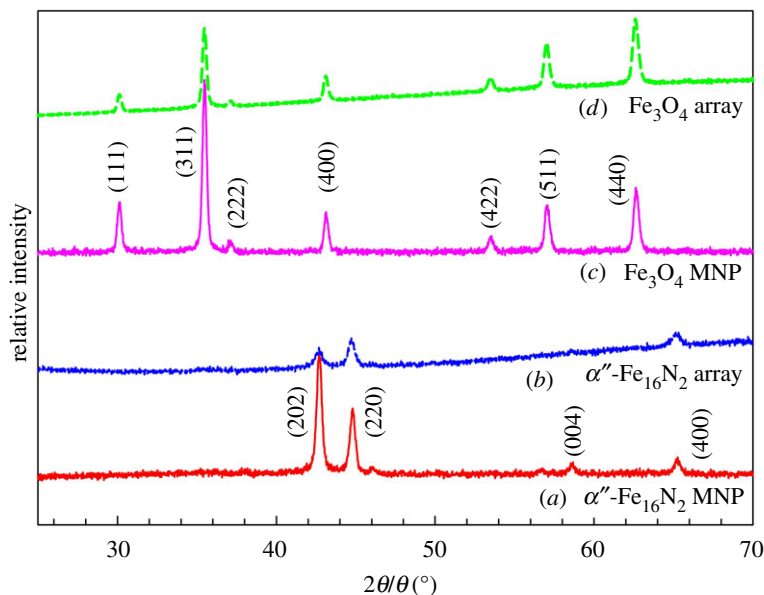


Figure 4. XRD patterns of (a) core-shell α'' - $\text{Fe}_{16}\text{N}_2/\text{Al}_2\text{O}_3$ MNPs and (b) their assembled arrays, (c) Fe_3O_4 MNPs and (d) their assembled arrays.

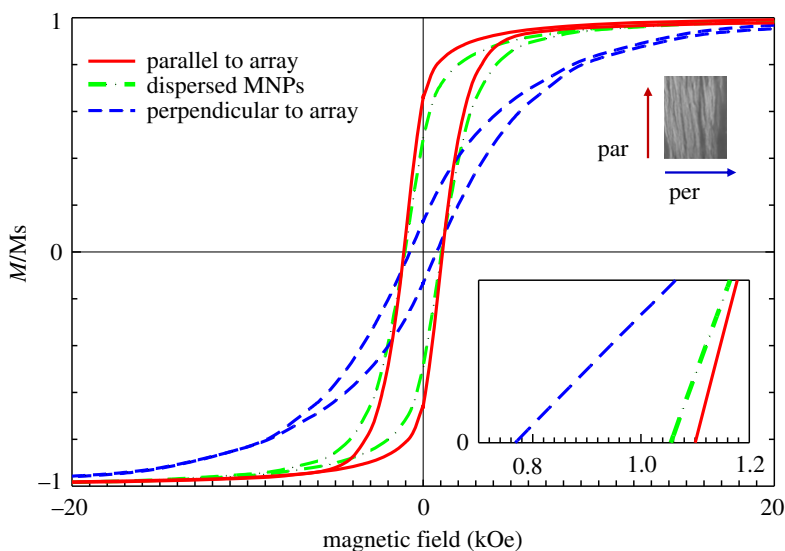


Figure 5. Magnetic characterization of dispersed core-shell α'' - $\text{Fe}_{16}\text{N}_2/\text{Al}_2\text{O}_3$ MNPs and their assembled array under an EMF of 15 T with the measured magnetic field applied parallel and perpendicular to arrays.

3.2. Magnetic property of arrays

Figure 5 shows the magnetic hysteresis (M - H) loops of the dispersed α'' - $\text{Fe}_{16}\text{N}_2/\text{Al}_2\text{O}_3$ MNPs and aligned arrays with the measured magnetic field parallel and perpendicular to the wire direction. These loops were obtained by SQUID measurements at 300 K. The magnetization (M) of each M - H loop is normalized by its corresponding saturation magnetization (M_s). The M_s for the fabricated array including the fabricated epoxy resin was 181 emu g^{-1} . Compared with the dispersed α'' - Fe_{16}N_2 MNPs, the shape of the M - H loop for the fabricated α'' - Fe_{16}N_2 array appeared to be more rectangular and spindle-shaped when the measured field was applied parallel and perpendicular to the array direction, respectively, as clearly shown in figure 5. The ratios of remanence (M_r) values and M_s were 49%, 66% and 13% for the dispersed α'' - Fe_{16}N_2 MNPs, arrays in the parallel and arrays in the perpendicular directions, respectively. The magnetic coercivity (H_c) values were 1.053, 1.120 and 0.766 kOe for the three cases, respectively. The characteristics of the M - H loops suggest that the

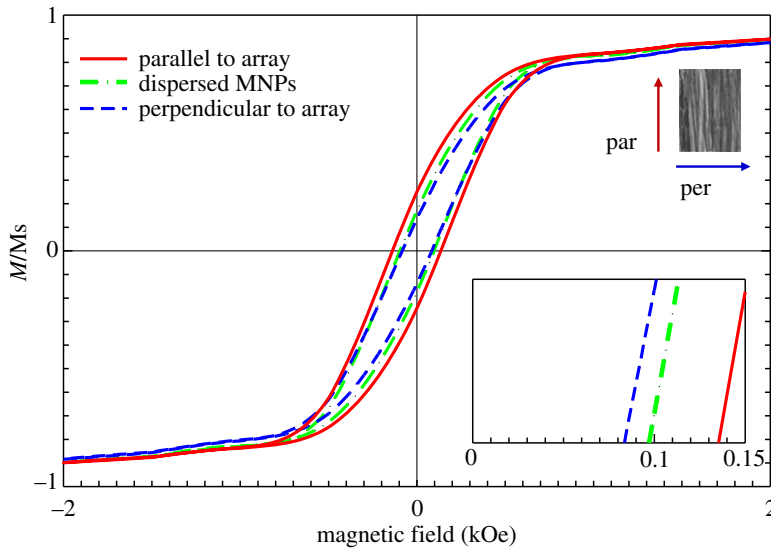


Figure 6. Magnetic characterization of dispersed Fe_3O_4 MNPs and their assembled array under an EMF of 15 T with the measured magnetic field applied parallel and perpendicular to arrays.

Table 1. Summary of magnetic properties at 300 K for dispersed $\alpha''\text{-Fe}_{16}\text{N}_2/\text{Al}_2\text{O}_3$ and Fe_3O_4 MNPs and their assembled arrays under an EMF of 15 T with the measured magnetic field applied parallel and perpendicular to arrays.

array	EMF direction	M_r/M_s (%)	H_c (kOe)
Fe_{16}N_2	particles	49	1.05
	parallel	66	1.12
	perpendicular	13	0.77
Fe_3O_4	particles	19	0.097
	parallel	26	0.136
	perpendicular	14	0.083

fabricated $\alpha''\text{-Fe}_{16}\text{N}_2$ wires exhibit enhanced magnetic properties along the wire direction with a larger M_s , M_r/M_s and H_c values than those of the dispersed MNPs and those in the vertical direction of the wires. The anisotropy field, calculated from the measured MNP easy axis (parallel to arrays) and hard axis (perpendicular to arrays) loops of the reduced magnetization [56], is 6.235 kOe for the $\alpha''\text{-Fe}_{16}\text{N}_2/\text{Al}_2\text{O}_3$ arrays. Although the increase in M_r/M_s and H_c is only 34.7% and 6.4% for the dispersed $\alpha''\text{-Fe}_{16}\text{N}_2/\text{Al}_2\text{O}_3$ MNPs, respectively, the result identifies that the used fabrication method is valid in producing arrays and enhancing their magnetic properties.

Figure 6 shows similar magnetic properties of fabricated Fe_3O_4 arrays to that of the $\alpha''\text{-Fe}_{16}\text{N}_2/\text{Al}_2\text{O}_3$ arrays, although the Fe_3O_4 MNPs show less magnetic anisotropy. The M_s value for the fabricated Fe_3O_4 array was 65 emu g^{-1} . The ratios of M_r/M_s were 19%, 26% and 14% for the dispersed Fe_3O_4 MNPs, arrays in the parallel and perpendicular directions, respectively, while the H_c values were approximately 0.097, 0.136 and 0.083 kOe for the three cases. The anisotropy field for the Fe_3O_4 arrays is 0.202 kOe, which is much lower than that of the $\alpha''\text{-Fe}_{16}\text{N}_2/\text{Al}_2\text{O}_3$ arrays. Thus, there is less difference for the hysteresis loops with the magnetic field applied in the directions perpendicular and parallel to the Fe_3O_4 arrays than that to the $\alpha''\text{-Fe}_{16}\text{N}_2/\text{Al}_2\text{O}_3$ arrays, as well as less coupled NPs in figure 3f. The characteristics of Fe_3O_4 $M-H$ loops were consistent with that of the $\alpha''\text{-Fe}_{16}\text{N}_2$ $M-H$ loops. This further identifies that the magnetic properties of the fabricated wires were enhanced by the EMF of 15 T. However, compared with the enhancement for the Fe_3O_4 array, the enhancement for the $\alpha''\text{-Fe}_{16}\text{N}_2/\text{Al}_2\text{O}_3$ arrays was much larger, owing to the higher isotropic of $\alpha''\text{-Fe}_{16}\text{N}_2/\text{Al}_2\text{O}_3$ MNPs than that of Fe_3O_4 MNPs. Magnetic properties at 300 K for dispersed $\alpha''\text{-Fe}_{16}\text{N}_2/\text{Al}_2\text{O}_3$ and Fe_3O_4 MNPs and their assembled arrays are summarized in table 1.

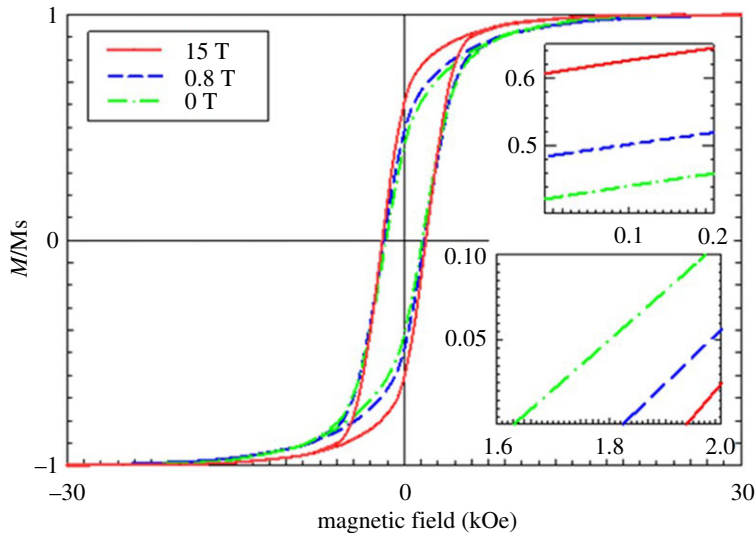


Figure 7. Magnetic characterization of dispersed spindle $\alpha''\text{-Fe}_{16}\text{N}_2/\text{Al}_2\text{O}_3$ MNPs and their assembled arrays under EMFs of 0.8 and 15 T with the measured magnetic field applied parallel to arrays.

Magnetic properties at 300 K for dispersed $\alpha''\text{-Fe}_{16}\text{N}_2/\text{Al}_2\text{O}_3$ and Fe_3O_4 MNPs and their assembled arrays are summarized in table 1. The application of a strong EMF with an intensity of 15 T has been demonstrated to be an effective approach to fabricate magnetic arrays from typical nanoparticles with high and low magnetic anisotropy, i.e. $\alpha''\text{-Fe}_{16}\text{N}_2/\text{Al}_2\text{O}_3$ and Fe_3O_4 MNPs.

The induced magnetic field strength of the arrays fabricated from $\alpha''\text{-Fe}_{16}\text{N}_2/\text{Al}_2\text{O}_3$ and Fe_3O_4 MNPs was directly measured using a magnetometer (TM-801, Kanetec, Japan). The magnetic values under the bottom of inner beakers used for fabrication were approximately 0.2 T and higher than the detection lower limit (less than 0.1 T). The generated detectable magnetic field suggests that the fabricated arrays from isotropic MNPs possess the potential application in tiny magnets [57].

3.3. Arrays fabricated from spindle-shaped MNPs

The fabricated wires possess a shape anisotropy and cause the difference of the magnetic performance in the parallel and perpendicular directions of the wires. The enhancement of magnetic properties for the fabricated straight wires in the parallel direction of the wires is due to the increased magnetic dipole-dipole interaction between MNPs in the wire direction [37]. In a new scenario, if elongated MNPs with shape anisotropy can rotate freely in a solvent, an EMF can make them orient along a magnetic easy axis oriented to the magnetic line and inevitably induce the formation of arrays. Thus, the shape anisotropy of MNPs can increase the alignment of single-domain MNPs with magnetic easy axes under an EMF [37,58]. The shape anisotropy will be enhanced if the external magnetic field is applied to spindle-shape MNPs.

Figure 7 presents the comparison of the magnetic property for the dispersed spindle-shape core-shell $\alpha''\text{-Fe}_{16}\text{N}_2/\text{Al}_2\text{O}_3$ MNPs and their aligned arrays under EMFs of 0.8 and 15 T with the magnetic field, as measured by SQUID, parallel to the wire direction. The magnetic properties of the spindle-shaped $\alpha''\text{-Fe}_{16}\text{N}_2/\text{Al}_2\text{O}_3$ MNPs 110 nm in length and 18 nm in width have been described in detail elsewhere [46]. The ratio of M_r/M_s and H_c increased with the EMF strength, as summarized in table 2. The increase in EMF strength caused the increase in the alignment of MNPs in arrays and resulted in an enhancement of magnetic performance of the fabricated arrays. This result is consistent with our previous report on the alignment of $\alpha''\text{-Fe}_{16}\text{N}_2/\text{Al}_2\text{O}_3$ MNPs in polymer films [54], as well as other investigations on the EMF intensity effect on wire-like structures via the direct synthesis under a weak EMF (less than 0.5 T) [33,51,59–61] and strong EMF (less than 1.4 T; 0–10 T) [8].

The ratio of M_r/M_s increased 15.0% and 44.4% under 0.8 and 15 T, respectively, while the H_c increased 11.7% and 19.0% for the two cases, respectively. The increase in M_r/M_s and H_c for the spindle-shaped $\alpha''\text{-Fe}_{16}\text{N}_2/\text{Al}_2\text{O}_3$ are both higher than those for the cube-like one (34.7% and 6.4%) under the same EMF of 15 T. The increased enhancement of magnetic properties is due to the spindle-shape anisotropy, which increases the alignment of single-domain MNPs along the EMF direction.

Table 2. Summary of magnetic properties at 300 K for the arrays assembled from spindle-shape α'' -Fe₁₆N₂/Al₂O₃ MNPs under EMF of 0.8 and 15 T with the measured magnetic field applied parallel to the arrays.

EMF intensity (T)	Mr/Ms (%)	Hc (kOe)
0	42.1	1.63
0.8	48.4	1.82
15	60.8	1.94

4. Conclusion

Magnetic arrays composed of highly dense wires have been successfully fabricated from well-dispersed cube-like Fe₃O₄ and core-shell cube/spindle-shaped α'' -Fe₁₆N₂/Al₂O₃ MNPs under an EMF of 15 T. The length and the aspect ratio of the fabricated arrays are of the order of 1 mm and 1000, respectively. The fabricated arrays possess enhanced magnetic properties along the wire direction compared with the dispersed MNPs. The comparison study of *M*–*H* loops reveals that the Mr/Ms and Hc values along the wire direction are both significantly higher than those of the MNPs. Compared with the cube-like α'' -Fe₁₆N₂/Al₂O₃ MNPs, the spindle-shaped ones have the advantage in the enhancement of magnetic performance of their fabricated arrays owing to the shape anisotropy. Compared with the Fe₃O₄ MNPs with low magnetic anisotropy, the assembled arrays from highly isotropic α'' -Fe₁₆N₂/Al₂O₃ MNPs generate a detectable magnetic field of approximately 0.2 T. These results indicate that the developed technique is feasible to fabricate magnetic wires in highly dense arrays at a large scale for various potential applications.

Data accessibility. The data for XRD and magnetic hysteresis loops are provided as electronic supplementary material. **Authors' contributions.** Q.L., T.I. and K.O. designed the research. K.O. and T.O. supervised the research. Q.L., C.W.K. and T.I. performed the experiments. Q.L. and C.W.K. contributed new reagents/analytic tools. Q.L., C.W.K. and K.O., with inputs from other co-authors, performed data analysis and wrote the paper.

Competing interests. The authors declare that there are no competing interests involved.

Funding. This work was supported by JSPS (Japan Society for the Promotion of Science) KAKENHI (grant nos. 26709061 and 16K13642). This work was partly supported by the Center for Functional Nano Oxide at Hiroshima University (Japan).

Acknowledgements. The authors thank Prof. Yoshihisa Fujiwara and Associate Prof. Takahiro Onimaru of Hiroshima University for the assistance in operating the superconducting magnet and performing the SQUID measurements.

References

- Krajewski M. 2017 Magnetic-field-induced synthesis of magnetic wire-like micro- and nanostructures. *Nanoscale* **9**, 16 511–16 545. (doi:10.1039/c7nr05823c)
- Nie ZH, Petukhova A, Kumacheva E. 2010 Properties and emerging applications of self-assembled structures made from inorganic nanoparticles. *Nat. Nanotechnol.* **5**, 15–25. (doi:10.1038/Nnano.2009.453)
- Allwood DA, Xiong G, Faulkner CC, Atkinson D, Petit D, Cowburn RP. 2005 Magnetic domain-wall logic. *Science* **309**, 1688–1692. (doi:10.1126/science.1108813)
- Sahoo Y, Cheon M, Wang S, Luo H, Furlani EP, Prasad PN. 2004 Field-directed self-assembly of magnetic nanoparticles. *J. Phys. Chem. B* **108**, 3380–3383. (doi:10.1021/jp031148i)
- Fratila RM, Rivera-Fernandez S, de la Fuente JM. 2015 Shape matters: synthesis and biomedical applications of high aspect ratio magnetic nanomaterials. *Nanoscale* **7**, 8233–8260. (doi:10.1039/c5nr01100k)
- Ivanov YP, Vazquez M, Chubykalo-Fesenko O. 2013 Magnetic reversal modes in cylindrical nanowires. *J. Phys. D: Appl. Phys.* **46**, 485001–485011. (doi:10.1088/0022-3727/46/48/485001)
- Ivanov YP, Alfidhel A, Alnassar M, Perez JE, Vazquez M, Chuvilin A, Kosel J. 2016 Tunable magnetic nanowires for biomedical and harsh environment applications. *Sci. Rep.-UK* **6**, 24 189–24 198. (doi:10.1038/Srep24189)
- Soumare Y, Dakhlaoui-Omrani A, Schoenstein F, Mercone S, Viau G, Jouini N. 2011 Nickel nanofibers and nanowires: elaboration by reduction in polyol medium assisted by external magnetic field. *Solid State Commun.* **151**, 284–288. (doi:10.1016/j.ssc.2010.12.004)
- Yan C, Wang T. 2017 A new view for nanoparticle assemblies: from crystalline to binary cooperative complementarity. *Chem. Soc. Rev.* **46**, 1483–1509. (doi:10.1039/c6cs00696e)
- Kavaldzhiev M, Perez JE, Ivanov Y, Bertoncini A, Liberale C, Kosel J. 2017 Biocompatible 3D printed magnetic micro needles. *Biomed. Phys. Eng. Expr.* **3**, 025005–025013. (doi:10.1088/2057-1976/Aa5ccb)
- Parkin SSP, Hayashi M, Thomas L. 2008 Magnetic domain-wall racetrack memory. *Science* **320**, 190–194. (doi:10.1126/science.1145799)
- Kim KJ *et al.* 2017 Energy-efficient writing scheme for magnetic domain-wall motion memory. *Appl. Phys. Exp.* **10**, 043002–043005. (doi:10.7567/Apex.10.043002)
- Ivanov YP, Chuvilin A, Lopatin S, Kosel J. 2016 Modulated magnetic nanowires for controlling domain wall motion: toward 3D magnetic memories. *ACS Nano*. **10**, 5326–5332. (doi:10.1021/acsnano.6b01337)
- Hoop M *et al.* 2018 Mobile magnetic nanocatalysts for bioorthogonal targeted cancer therapy. *Adv. Funct. Mater.* **28**, 1705920–1705927. (doi:10.1002/adfm.201705920)
- Thorkelsson K, Bai P, Xu T. 2015 Self-assembly and applications of anisotropic nanomaterials: a review. *Nano Today* **10**, 48–66. (doi:10.1016/j.nantod.2014.12.005)

16. Boles MA, Engel M, Talapin DV. 2016 Self-assembly of colloidal nanocrystals: from intricate structures to functional materials. *Chem. Rev.* **116**, 11 220–11 289. (doi:10.1021/acs.chemrev.6b00196)
17. Wang H, Li M, Li XY, Xie KN, Liao L. 2015 Preparation and thermal stability of nickel nanowires via self-assembly process under magnetic field. *Bull. Mater. Sci.* **38**, 1285–1289. (doi:10.1007/s12034-015-1012-y)
18. Tang SC, Zheng Z, Vongehr S, Meng XK. 2011 Facile and rapid synthesis of nickel nanowires and their magnetic properties. *J. Nanopart. Res.* **13**, 7085–7094. (doi:10.1007/s11051-011-0622-6)
19. Li M, Xie KA, Wu YZ, Yang QX, Liao L. 2013 Synthesis of cobalt nanowires by template-free method. *Mater. Lett.* **111**, 185–187. (doi:10.1016/j.matlet.2013.08.088)
20. Ung D, Viau G, Ricolleau C, Warmont F, Gredin P, Fievet FF. 2005 CoNi nanowires synthesized by heterogeneous nucleation in liquid polyol. *Adv. Mater.* **17**, 338–344. (doi:10.1002/adma.200400915)
21. Xia YN, Yang PD, Sun YG, Wu YY, Mayers B, Gates B, Yin YD, Kim F, Yan YQ. 2003 One-dimensional nanostructures: synthesis, characterization, and applications. *Adv. Mater.* **15**, 353–389. (doi:10.1002/adma.200390087)
22. Hinaut A *et al.* 2018 Electro spray deposition of structurally complex molecules revealed by atomic force microscopy. *Nanoscale* **10**, 1337–1344. (doi:10.1039/c7nr02621c)
23. Thongmee S, Pang HL, Ding J, Lin JY. 2009 Fabrication and magnetic properties of metallic nanowires via AAO templates. *J. Magn. Magn. Mater.* **321**, 2712–2716. (doi:10.1016/j.jmmm.2009.03.074)
24. Yang HZ, Li Y, Zeng M, Cao W, Bailey WE, Yu RH. 2016 Static and dynamic magnetization of gradient FeNi alloy nanowire. *Sci. Rep.-UK* **6**, 20 427–20 435. (doi:10.1038/Srep20427)
25. Zhang XL, Zhang HM, Wu TS, Li ZY, Zhang ZJ, Sun HY. 2013 Comparative study in fabrication and magnetic properties of FeNi alloy nanowires and nanotubes. *J. Magn. Magn. Mater.* **331**, 162–167. (doi:10.1016/j.jmmm.2012.11.033)
26. Wang ML, Wu ZG, Yang H, Liu YN. 2018 Growth orientation control of Co nanowires fabricated by electrochemical deposition using porous alumina templates. *Cryst. Growth Des.* **18**, 479–487. (doi:10.1021/acs.cgd.7b01464)
27. Zhu XX, Fan JX, Zhang Y, Zhu H, Dai B, Yan MH, Ren Y. 2017 Preparation of superparamagnetic and flexible gamma-Fe₂O₃ nanowire arrays in an anodic aluminum oxide template. *J. Mater. Sci.* **52**, 12 717–12 723. (doi:10.1007/s10853-017-1383-0)
28. Wu W, Xiao XH, Zhang SF, Zhou JA, Fan LX, Ren F, Jiang CZ. 2010 Large-scale and controlled synthesis of iron oxide magnetic short nanotubes: shape evolution, growth mechanism, and magnetic properties. *J. Phys. Chem. C* **114**, 16 092–16 103. (doi:10.1021/jp1010154)
29. Li Y, Shen WJ. 2014 Morphology-dependent nanocatalysts: rod-shaped oxides. *Chem. Soc. Rev.* **43**, 1543–1574. (doi:10.1039/c3cs60296f)
30. Scott JA, Totonjian D, Martin AA, Tran TT, Fang JH, Toth M, McDonagh AM, Aharonovich I, Lobo CJ. 2016 Versatile method for template-free synthesis of single crystalline metal and metal alloy nanowires. *Nanoscale* **8**, 2804–2810. (doi:10.1039/c5nr07307c)
31. Soumare Y, Garcia C, Maurer T, Chaboussant G, Ott F, Fievet F, Piquemal JY, Viau G. 2009 Kinetically controlled synthesis of hexagonally close-packed cobalt nanorods with high magnetic coercivity. *Adv. Funct. Mater.* **19**, 1971–1977. (doi:10.1002/adfm.200800822)
32. Ouar N, Farhat S, Mercene S, Zighem F, Schoenstein F, Jouini N, Hinkov I, Wang G, Ricolleau C. 2015 Magnetic nanowire synthesis: a chemical engineering approach. *Aiche J.* **61**, 304–316. (doi:10.1002/aic.14605)
33. Sun LX, Chen QW, Tang Y, Xiong Y. 2007 Formation of one-dimensional nickel wires by chemical reduction of nickel ions under magnetic fields. *Chem. Commun.* **27**, 2844–2846. (doi:10.1039/b704689h)
34. Hu L, Zhang RR, Chen QW. 2014 Synthesis and assembly of nanomaterials under magnetic fields. *Nanoscale* **6**, 14 064–14 105. (doi:10.1039/c4nr05108d)
35. Zhang JQ, Xiang WF, Liu Y, Hu MH, Zhao K. 2016 Synthesis of high-aspect-ratio nickel nanowires by dropping method. *Nanoscale Res. Lett.* **11**, 118–222. (doi:10.1186/s11671-016-1330-Z)
36. Wang MS, He L, Yin YD. 2013 Magnetic field guided colloidal assembly. *Mater. Today* **16**, 110–116. (doi:10.1016/j.mattod.2013.04.008)
37. Lisjak D, Mertelj A. 2018 Anisotropic magnetic nanoparticles: a review of their properties, syntheses and potential applications. *Prog. Mater. Sci.* **95**, 286–328. (doi:10.1016/j.pmatsci.2018.03.003)
38. Wang MS, Yin YD. 2016 Magnetically responsive nanostructures with tunable optical properties. *J. Am. Chem. Soc.* **138**, 6315–6323. (doi:10.1021/jacs.6b02346)
39. Ge JP, Hu YX, Biasini M, Beyermann WP, Yin YD. 2007 Superparamagnetic magnetite colloidal nanocrystal clusters. *Angew. Chem. Int. Ed.* **46**, 4342–4345. (doi:10.1002/anie.200700197)
40. Wang MS, He L, Xu WJ, Wang X, Yin YD. 2015 Magnetic assembly and field-tuning of ellipsoidal-nanoparticle-based colloidal photonic crystals. *Angew. Chem. Int. Ed.* **54**, 7077–7081. (doi:10.1002/anie.201501782)
41. Ge JP, He L, Hu YX, Yin YD. 2011 Magnetically induced colloidal assembly into field-responsive photonic structures. *Nanoscale* **3**, 177–183. (doi:10.1039/c0nr00487a)
42. Sheparovych R, Sahoo Y, Motornov M, Wang SM, Luo H, Prasad PN, Sokolov I, Minko S. 2006 Polyelectrolyte stabilized nanowires from Fe₃O₄ nanoparticles via magnetic field induced self-assembly. *Chem. Mater.* **18**, 591–593. (doi:10.1021/cm051274u)
43. Ryan KM, Mastroianni A, Stancil KA, Liu HT, Alivisatos AP. 2006 Electric-field-assisted assembly of perpendicularly oriented nanorod superlattices. *Nano Lett.* **6**, 1479–1482. (doi:10.1021/nl060866o)
44. Kartikowati CW, Suhendi A, Zuhijah R, Ogi T, Iwaki T, Okuyama K. 2016 Preparation and evaluation of magnetic nanocomposite fibers containing α' -Fe₁₆N₂ and α -Fe nanoparticles in polyvinylpyrrolidone via magneto-electrospinning. *Nanotechnology* **27**, 025601–025610. (doi:10.1088/0957-4484/27/2/025601)
45. Kartikowati CW, Li Q, Horie S, Ogi T, Iwaki T, Okuyama K. 2017 Aligned Fe₃O₄ magnetic nanoparticle films by magneto-electrospray method. *RSC Adv.* **7**, 40 124–40 130. (doi:10.1039/c7ra07944c)
46. Ogi T, Li Q, Horie S, Tameka A, Iwaki T, Okuyama K. 2016 High-purity core-shell α' -Fe₁₆N₂/Al₂O₃ nanoparticles synthesized from α -hematite for rare-earth-free magnet applications. *Adv. Powder Technol.* **27**, 2520–2525. (doi:10.1016/j.apt.2016.09.017)
47. Li Q, Kartikowati CW, Horie S, Ogi T, Iwaki T, Okuyama K. 2017 Correlation between particle size/domain structure and magnetic properties of highly crystalline Fe₃O₄ nanoparticles. *Sci. Rep.-UK* **7**, 9894–9900. (doi:10.1038/S41598-017-09897-5)
48. Tahara T, Imajyo Y, Nandiyo ABD, Ogi T, Iwaki T, Okuyama K. 2014 Low-energy bead-milling dispersions of rod-type titania nanoparticles and their optical properties. *Adv. Powder Technol.* **25**, 1492–1499. (doi:10.1016/j.apt.2014.04.004)
49. Ogi T, Zuhijah R, Iwaki T, Okuyama K. 2017 Recent progress in nanoparticle dispersion using bead mill. *KONA Powder Part. J.* **34**, 3–23. (doi:10.14356/kona.2017004)
50. Sueda M, Katsuki A, Fujiwara Y, Tanimoto Y. 2006 Influences of high magnetic field on glycine crystal growth. *Sci. Technol. Adv. Mat.* **7**, 380–384. (doi:10.1016/j.stam.2006.02.006)
51. Sun Q, Wang SG, Wang RM. 2012 Well-aligned CoPt hollow nanochains synthesized in water at room temperature. *J. Phys. Chem. C* **116**, 5352–5357. (doi:10.1021/jp210144p)
52. Wang J, Chen QW, Zeng C, Hou BY. 2004 Magnetic-field-induced growth of single-crystalline Fe₃O₄ nanowires. *Adv. Mater.* **16**, 137–140. (doi:10.1002/adma.200306136)
53. Li Q, Kartikowati CW, Ogi T, Iwaki T, Okuyama K. 2017 Facile fabrication of carbon nanotube forest-like films via coaxial electro spray. *Carbon* **115**, 116–119. (doi:10.1016/j.carbon.2016.12.095)
54. Kartikowati CW, Suhendi A, Zuhijah R, Ogi T, Iwaki T, Okuyama K. 2016 Effect of magnetic field strength on the alignment of α' -Fe₁₆N₂ nanoparticle films. *Nanoscale* **8**, 2648–2655. (doi:10.1039/c5nr07859h)
55. Feng L, Jiang L, Mai Z, Zhu D. 2004 Polymer-controlled synthesis of Fe₃O₄ single-crystal nanorods. *J. Colloid Interface Sci.* **278**, 372–375. (doi:10.1016/j.jcis.2004.06.019)
56. Neudert A, McCord J, Schafer R, Schultz L. 2004 Dynamic anisotropy in amorphous CoZrTa films. *J. Appl. Phys.* **95**, 6595–6597. (doi:10.1063/1.1667796)
57. Song NN, Yang HT, Liu HL, Ren X, Ding HF, Zhang XQ, Cheng ZH. 2013 Exceeding natural resonance frequency limit of monodisperse

- Fe₃O₄ nanoparticles via superparamagnetic relaxation. *Sci. Rep.-UK* **3**, 3161–3165. (doi:10.1038/Srep03161)
58. Niu H, Chen Q, Ning M, Jia Y, Wang X. 2004 Synthesis and one-dimensional self-assembly of acicular nickel nanocrystallites under magnetic fields. *J. Phys. Chem. B* **108**, 3996–3999. (doi:10.1021/jp0361172)
59. Shen JY, Yao YT, Liu YJ, Leng JS. 2016 Tunable hierarchical Fe nanowires with a facile template-free approach for enhanced microwave absorption performance. *J. Mater. Chem. C* **4**, 7614–7621. (doi:10.1039/c6tc01912a)
60. Tang Y, Chen QW, Chen RS. 2015 Magnetic field induced controllable self-assembly of maghemite nanocrystals: from 3D arrays to 1D nanochains. *Appl. Surf. Sci.* **347**, 202–207. (doi:10.1016/j.apsusc.2015.04.066)
61. Li PW, Chen WM, Liu W, Li ZA, Cui YM, Huang AP, Wang RM, Chen CP. 2010 Thermodynamic phase formation of morphology and size controlled Ni nanochains by temperature and magnetic field. *J. Phys. Chem. C* **114**, 7721–7726. (doi:10.1021/jp912168h)